TABLE III. The differential cross section and asymmetry parameter for the case $Z=48$, $v/c=0.2$.

θ	15°	30°	45°	60°	75°	90°	105°	120°	135°	150°	165°
σ (barns)	2200	150	35	12	4.6	2.0	0.90	0.48	0.31	0.24	0.22
σ/σ_0	0.98	1.04	1.18	1.14	0.93	0.69	0.48	0.35	0.28	0.25	0.24
$100\,S(\theta)$	0.0	0.3	0.3	−0.5	−2	−4	−7	−10	−11	−9	−5
$100\,S_0(\theta)$	−0.0	0.4	1.2	0.08	−3.7	−8	−11	−12	−11	−8.2	−4.4

TABLE IV. The differential cross section and asymmetry parameter for the case $Z=48$, $v/c=0.4$.

θ	15°	30°	45°	60°	75°	90°	105°	120°	135°	150°	165°
σ (barns)	130	8.6	1.5	0.37	0.10	0.031	0.010	0.0044	0.0027	0.0023	0.0022
σ/σ_0	1.05	1.04	0.83	0.56	0.34	0.18	0.098	0.059	0.047	0.048	0.052
$100\,S(\theta)$	0.06	−0.2	−0.9	−1.6	−2	−3	−5	−9	−14	−13	−8
$100\,S_0(\theta)$	0.2	0.2	−1.2	−4.3	−8.3	−12	−15	−16	−15	−12	−6.3

fact polarization effects are expected to be large. The cross section falls off sharply with increasing energy, particularly for a finite-size nucleus so that measurements of μ-meson scattering above 10 Mev would be extremely difficult.

ACKNOWLEDGMENT

The authors wish to thank Watson Scientific Computing Laboratories for the use of their computing machine IBM type 650.

PHYSICAL REVIEW VOLUME 111, NUMBER 1 JULY 1, 1958

Scattering of 220-Mev Polarized Protons by Complex Nuclei*

E. M. HAFNER
University of Rochester, Rochester, New York
(Received January 27, 1958)

Extending earlier measurements, we have studied yields and asymmetries in the scattering of a highly polarized proton beam by Be^9, C^{12}, Al^{27}, and Ca^{40}. In the work on Be^9 and Al^{27}, the beam was monochromatized through the use of a regenerative deflector; its mean energy on striking the targets was 219.6 Mev, and its standard deviation in energy (including the effect of short time fluctuations) was less than 1.1 Mev. With this technique, together with a refined procedure for the analysis of the distribution in range of scattered protons, we have been able to separate elastic from inelastic scattering in Be^9 at angles from 8° to 37.5°, and to estimate the inelastic scattering involving the excited state at 2.4 Mev. The separation of elastic scattering in Ca^{40} could also be made, although the regenerator was not used. The results are compared with approximate calculations based on the optical model with $\boldsymbol{\sigma}\cdot\mathbf{L}$ coupling; a potential is found such that, with variation of the nuclear radius alone, good fits are obtained to measurements on the four nuclei.

INTRODUCTION

POLARIZATION effects in the elastic scattering of high-energy protons have been studied intensively at this laboratory[1] and elsewhere[2] over an energy interval extending from 60 Mev to 660 Mev. It has become clear from the experiments that the polarization can be very large, and can in fact approach 100% under certain conditions. The first strong maximum in the function $P(\theta)$ is usually found when $2kR\sin(\theta/2)\simeq 2.2$, k and θ being the wave number and scattering angle in the center-of-mass system, and R the nuclear radius. Some experiments[1,3] have also revealed subsequent minima and maxima in $P(\theta)$ at large angles, but only after careful elimination of inelastic events that can compete strongly with elastic scattering in the angular region beyond the first maximum in the polarization. Measurements in which such separation has been accomplished have given data on polarization effects involving one or more of the lowest excited states of the target nuclei.

Most theoretical accounts[2] of the qualitative features of the elastic polarization have been achieved through the addition of a spin-orbit term to the central potential of the usual optical model. It was the purpose of the present work to extend our original measurements at 220-Mev to a variety of nuclei, and then to investigate

* Research supported by the U. S. Atomic Energy Commission.
[1] Chesnut, Hafner, and Roberts, Phys. Rev. **104**, 449 (1956); referred to in the text of this paper as CHR.
[2] An excellent bibliography of most of the experimental and theoretical work in this field is found in the review article by L. Wolfenstein, *Annual Review of Nuclear Science* (Annual Reviews, Inc., Stanford, 1956), Vol. 6, p. 43.
[3] Alphonce, Johannson, and Tibell, Nuclear Phys. **3**, 185 (1957).

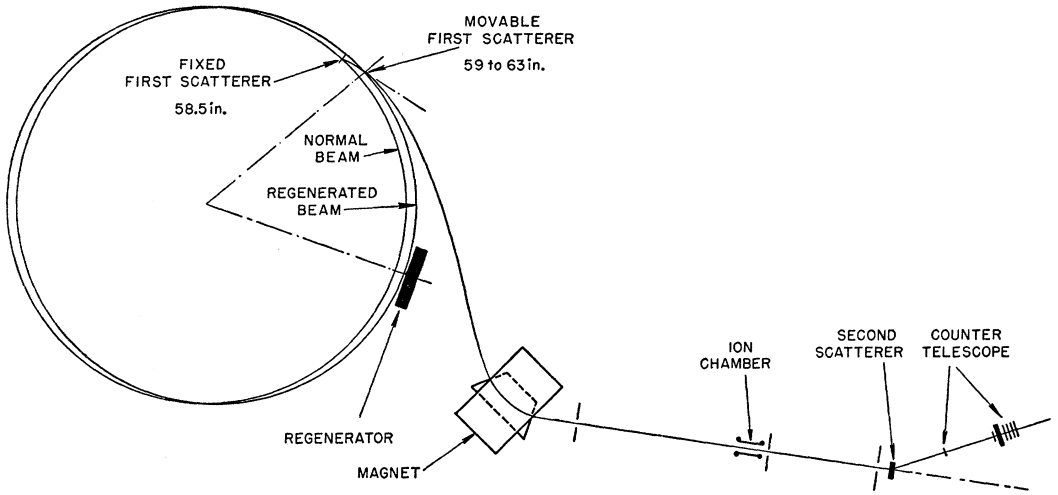

FIG. 1. Schematic plan of the double-scattering experiment.

the possibility of discovering a potential that gives quantitative descriptions of the elastic scattering in all cases. In carrying out the analysis, we wished specifically to stipulate that all parameters of the potential be held constant except for the range, which was to be varied in proportion to the nuclear radius. The nuclei chosen for the comparison were Be^9, C^{12}, Al^{27}, and Ca^{40}, giving a significant range of mass number and a variety of ground-state spins.

The separation of elastic from inelastic scattering at 220 Mev is the most formidable technical problem confronting us in this work. In Be^9, for example, the inelastically scattered group corresponding to excitation of the state at 2.4 Mev differs from the elastic group by only 1.0% in energy and 0.6% in momentum. The requirements for a successful study of the scattering, in the event that inelastic processes play a significant role, therefore include a narrow energy spread of the incident beam and a second-scattering detection procedure of high resolution. As will be seen in subsequent discussion, we have been able to achieve the necessary sharpness in beam energy by regenerative deflection of the cyclotron beam before the first scattering. In the hope of replacing the distribution-in-range methods developed in CHR for detection of second scattering, we investigated the response of several scintillation spectrometers to this beam and concluded that, with the detectors of this type available to us at present, the required resolution cannot be achieved. At the same time it became apparent, from independent work[3,4] on C^{12} at lower energy, that the polarization data reported in CHR is in excellent agreement with the results of more direct methods. (Figure 16 shows a comparison of the results for inelastic scattering.) In view of this agreement, and of the improvement in incident energy definition that had become available to us, we were encouraged to devise a refinement of our previous methods that could be expected to cope with some more difficult problems.

[4] Tyren, Hillman, and Johannson, Nuclear Phys. **3**, 336 (1957).

FIRST-SCATTERED REGENERATED BEAM

Following the theoretical work[5] of Le Couteur on the regenerative deflection of synchrocyclotron beams, we undertook an investigation of the technique with our machine. Careful measurement of the cyclotron magnetic field and a study of Le Couteur's nonlinear theory led us to devise regenerator parameters and to develop semiempirical methods[6] for designing the physical regenerator and its correcting shims with a minimum of down-time on the machine. The regenerator was successfully tested, with the conclusion that about 30% of the circulating beam could be deflected into an area representing the entrance of a proposed magnetic channel. At the same time we were made aware, from results with similar apparatus at other laboratories, that the deflected beams were considerably sharper in energy than the circulating beams from which they arose. Now, the best *extracted* currents available in these machines were about 5% of internal currents; it was therefore possible that at least some of the improvement in energy definition was the result of momentum selection in magnetic channels. Since it was also at this time that the importance of energy resolution in double nuclear scattering became clear, we thought it interesting to look at the energy spread of our regenerated beam *before* extraction.

The method used for this investigation is shown in Fig. 1. A polarized proton beam is normally produced by 15-degree scattering from a fixed first scatterer at a radius of 58.5 inches. After traversing a steering magnet, a monitoring ionization chamber, and several defining slits, it is analyzed by a second scatterer and a counter

[5] K. J. Le Couteur, Proc. Phys. Soc. (London) **B64**, 1073 (1951); **66**, 25 (1953); Phil. Mag. Ser. 7, **46**, 1265 (1955).
[6] E. M. Hafner and K. J. Le Couteur (unpublished).

telescope. With the regenerator in place, the first scatterer was made movable through a suitable range of radii, and along a line closely approximating the usual scattered orbit. The similarity of scattering angles and subsequent ion optics for all target positions made possible a realistic comparison between the normal scattered flux and the flux obtainable under a given condition of regeneration. In addition, the analyzer telescope was equipped to measure distributions in range and in time of particles reaching the second scatterer, and thus to give comparisons of energy spread and duty cycle between the two beams.

Curve A of Fig. 2 is a Gaussian fit to the distribution in energy deduced from a typical range measurement on a double scattered unregenerated beam. The energy scale refers to the beam striking the first target. Curve B is a fit to a range measurement on a beam that had undergone regeneration before the first scattering. The standard deviation used in drawing this curve is taken from a calculation of the straggling to be expected in the absorbers of the analyzer telescope, and in residual thicknesses of material (targets, counters, and air) through which the beam passed. It is clear that the beam itself contributes little to the width of the distribution. The departure of the data from the curve on the low-energy side is attributed to inelastic scattering at the first target, which was carbon. The dotted correction to the curve shows the effect of assuming a 7% admixture of scattering involving 4.4-Mev excitation of C^{12}. A contamination of approximately this amount might be expected from the fact that the Uppsala group[7] has obtained a corresponding figure of 10% for 16-degree scattering at 155 Mev.

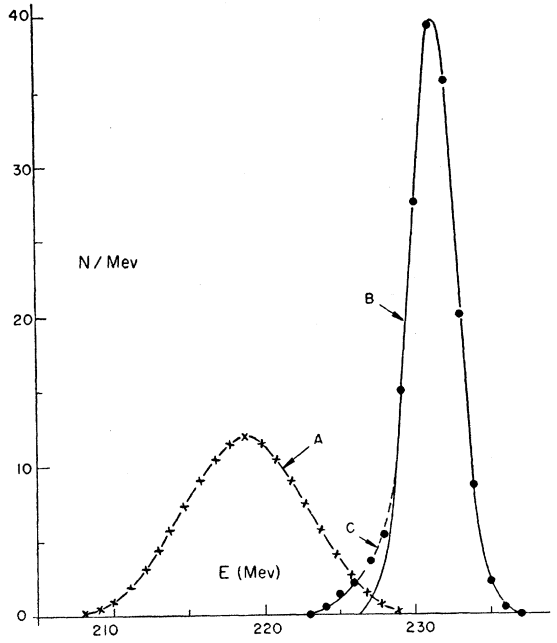

FIG. 2. Differential range data. The absorber thickness for each measurement is the mean range corresponding to the energy at which the point is plotted. The points on curve A were obtained with the normal cyclotron beam; those on B with the regenerated beam. Curve B is the expectation from straggling in range. The correction shown as C takes account of inelastic scattering by the first target (see text).

The total flux observed in the regenerated beam by this method indicated no loss due to regeneration; indeed, the integral of B in Fig. 2 exceeds the integral of A by about 20%. We believe this to suggest that the energy spread of the normal beam is in fact greater than the measurement in second scattering indicates, and that the steering magnet serves to some extent as an analyzer.

The distributions in time of the two beams also revealed a striking difference. The measurements were made by observing the number of second scatterings that occurred within a 6-microsecond gate opened at variable times after the cyclotron oscillator passed a preset frequency near the bottom of the FM envelope. The distribution corresponding to curve A of Fig. 2 was about 60 microseconds wide at half-maximum, and correlation was found between time of arrival of a proton and its range. The distribution of the regenerated beam was 24 microseconds wide, and showed no range correlation. Also, a width of 80 microseconds was observed for neutrons produced by the unregenerated beam. Since the entire circulating beam contributed to this distribution, the increase in width suggests once more that the steering magnet and slit system reject part of the proton spectrum.

From range data accumulated during these experiments, interpreted by means of procedures discussed in the following section, we have deduced the mean energy of protons at each of several points along the beam. With the regenerator in operation, the energy striking the first target is 231.1 Mev; the energy leaving the target is 223.4 Mev; the energy at the steering magnet is 221.5 Mev; and the energy striking the second target is 219.5 Mev. Departures of the energy from the mean were seldom greater than 0.3 Mev. The polarization of the first-scattered beam was reported in CHR as 0.89 ± 0.02. Remeasurements of the polarization during the present work have confirmed this result.

The flux available to us in the first-scattered beam can be computed from a knowledge of the p-C^{12} cross section and of the subsequent ion optics. A study of orbits carried out on a Burroughs E-101 computer indicates that the mean ray accepted externally is produced by scattering at 14.7 degrees, and that the solid angle determined by external apertures is 7.5×10^{-5} steradian at the target. Using a differential cross section for C^{12} obtained from analysis of the data in CHR, we compute a flux of 2.3×10^{8} protons/min for a circulating beam of 0.3 microampere, the current at present available. The flux calibration has been confirmed with fair accuracy by the counting rates obtained in several independent

[7] A. Johannson *et al.*, Nuclear Phys. (to be published).

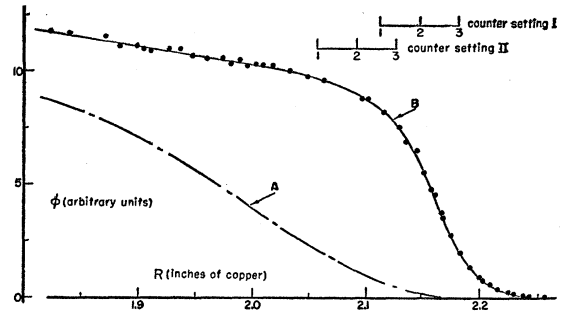

FIG. 3. Integral range data. Curve A is taken from the earlier work of CHR. Curve B was obtained in the present work with the regenerated beam. Also shown are two range settings of the counter telescope used in the present measurements on Be^9.

double-scattering measurements, and by direct measurement[8] of the flux density with small counters.

DOUBLE SCATTERING TECHNIQUE

The basic procedure used in the present measurements is a refinement of the ideas developed in CHR. We shall emphasize in this discussion only such aspects of the method as have been significantly changed. It is usually to be assumed that the regenerated beam was used to produce a first scattering although some of our data were obtained with the normal beam. Our starting point was a carefully measured integral range curve, taken either in the first-scattered beam or in the second-scattered beam at a small angle. We found good agreement between the two curves if, for example, the second scatterer was Be^9 and the second angle was less than 8 degrees; at larger angles, inelastic scattering introduced significant changes. Figure 3 shows the range curve used in analysis of the asymmetry measurements, and includes data taken over a period of time comparable with the length of asymmetry runs. It therefore includes the broadening contributed by random energy fluctuations. The curve is a fit to the data, obtained by combining a gaussian centered at the full energy with a 7% admixture centered at an energy lower by 4.4 Mev. The contribution of the incident beam energy spread to the standard deviation of the Gaussians is less than 1.1 Mev. The admixture of energies is in conformity with the results of differential range measurements (Fig. 2); it is also found to be required for an adequate fit. Nuclear absorption and geometrical losses were taken into account by an empirical factor, adjusted to the slope of the range curve ahead of the final falloff. Included for comparison in Fig. 3 is the integral range curve of the unregenerated beam used in the measurements of CHR and in the Ca^{40} measurements of the present report; its standard deviation is about three times as large.

The telescope used in detection of second scattering consisted of five counters (Fig. 4), whose signals were detected in conventional coincidence circuitry. The function of the first two counters was only to define the solid angle of acceptance, which was approximately 0.005 steradian. The last three, which we shall denote by 1–2–3, were thin plastic scintillators (0.16 g/cm^2; energy loss 0.9 Mev at 220 Mev) between which thin absorbers could be placed in order to space the counters appropriately on the range curve. In front of these three counters we placed a thick copper absorber chosen, for a given angle of scattering from a given target, to make up a total copper equivalent thickness R_1 (measured in inches) between the cyclotron beam and counter 1. The absorber was adjusted in every run to take into account energy losses due to ionization and nuclear recoil in the second scatterer, and thus to guarantee that the distribution-in-range of elastically scattered protons arriving at counter 1 was at least approximately the same for all measurements. In careful analysis of the data, it was then necessary only to correct for small deviations of the primary energy from the value corresponding to the standard range curve of Fig. 3. The extent of such deviations, and the way in which they were accounted for, will be described presently.

The thin absorbers placed between the last three counters were chosen so that ΔR, the increment in range between successive counters, corresponded to the energy loss for inelastic scattering leaving a nucleus of the second scatterer in its first excited state. ΔR, measured again as an equivalent copper thickness in inches, includes the thickness of one counter. Calibrations of the relative efficiencies of the counters were made, so that the rates in counters 2 and 3 could be compared with the rate in counter 1. The efficiency of a counter relative to the preceding one was found to be about 90% when ΔR was set for an energy increment of 2.4 Mev, appropriate to the case of Be^9. When the efficiency correction had been made, the relative rates for elastic scattering into the three counters could be compared with what was expected from the range curve of Fig. 3. In our procedure, it was this comparison that revealed rather precisely any possible deviations of the primary energy.

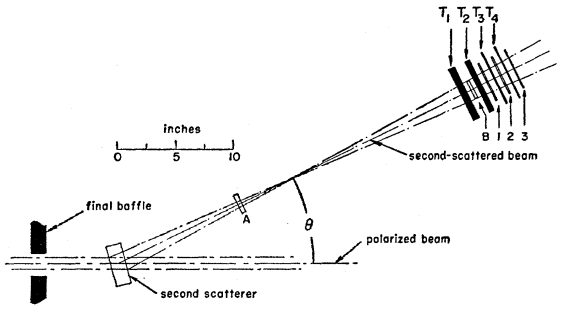

FIG. 4. Schematic plan of the second-scattering counter telescope, set for scattering to the left. The solid angle accepted by the counters is, for the narrow beam width shown here, determined by the target illumination and counter B; the angular resolution in θ is approximately 2.5°. T_1 and T_2 are thick absorbers; T_3 and T_4 are thin absorbers separating the $\frac{1}{16}$-inch scintillators 1, 2, and 3.

[8] Roberts, Tinlot, and Heer (private communication).

As an example of the way in which the primary energy can be monitored, consider the range settings denoted by I in Fig. 3. The total copper equivalent ahead of counter 1 is 2.119 inches, and the subsequent counters are separated by 0.035 inch of copper equivalent, corresponding to increments of 2.4 Mev at 220 Mev. We now adopt a notation introduced in CHR. Let ϕ_i be the rate (after correction for efficiency) in the ith counter and let ϕ_{ij}, with $j=i+1$, be the difference between the rates in i and j. Further, introduce the ratios $x_i=\phi_j/\phi_i$ and $x_{ij}=\phi_{jk}/\phi_{ij}$, with $k=j+1$; we impose the restriction that the x's are defined only when the telescope is in the first-scattered beam, or when it is detecting second scattering at an angle small enough to insure that inelastic events do not contribute significantly to the count. The three thin counters in our telescope can then give x_1, x_{12}, and x_2 directly. If, in a given run, the primary beam energy happened to be the same as the mean energy that led to our standard range curve, and if the spread in energy was also the same, then the observed ratios were expected to agree with those read from the curve of Fig. 3 at the actual range positions of the counters. But if, for example, the energy had drifted upward, we could expect ratios that corresponded to an apparent decrease of R_1; this shift could then be used to deduce the change in energy. We show in Fig. 5 the distribution of ratios observed in a sequence of runs on Be^9 at small angles. The curves are computed ratios, based upon the fit to the data of Fig. 3 and taken as functions of R_1. (The ratios x_{23} and x_3 are included for later reference.) The results of each small-angle run are plotted at the value of R_1 that gives the best fit to the curves; the upper scale then gives our best estimate of the primary energy at the time of each run. These runs covered a period of ten days, and it appears that the

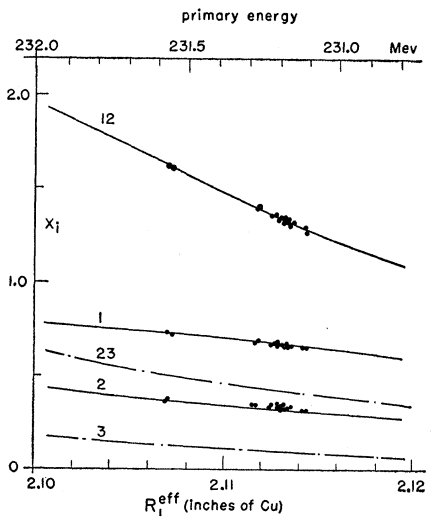

FIG. 5. Counter ratios, x_i, observed in small-angle scattering from Be^9. The curves are deduced from the range data B of Fig. 3. The effective R_1 and the primary energy for each run are found by fitting the data to the curves.

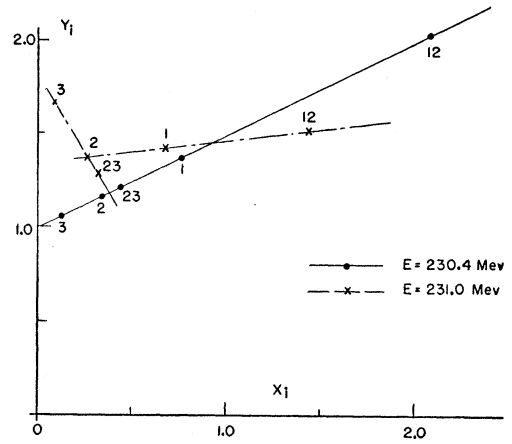

FIG. 6. Hypothetical Y_i *vs* x_i data. The solid line is obtained when energy and range are compatible; a small uncorrected shift of R_1, equivalent to a 0.6-Mev change in energy leads to the points on the dashed lines.

energy was remarkably stable during that time. It also appears from the accuracy with which most of the runs can be fitted, that the energy spread of the beam did not change significantly over the period of the measurements.

Since the most critical point in the analysis of our asymmetry measurements is concerned with a precise knowledge of primary energy, we have sought independent ways of verifying the correctness of the procedure outlined above. The most straightforward of our checks were made by varying the energy of the primary beam by predictable amounts, and observing corresponding changes in counter ratios. For example, we predict that an outward radial shift of the first scatterer by 0.15 inch will give an increase of 0.7 ± 0.2 Mev in energy, the uncertainty arising from lack of precise knowledge of the n value for the cyclotron field. When this shift was made, the counter ratios were observed to indicate an energy increase of 0.80 ± 0.05 Mev. In another test, the cyclotron field was raised by 0.23%, leading to an anticipated energy rise of 0.96 ± 0.05 Mev; the increase indicated by our counter technique was 0.93 ± 0.05 Mev. These checks have given us confidence in the sensitivity and the accuracy of our procedure.

Apart from refinements already mentioned, the steps taken in the reduction of our experimental data are similar to those described in CHR. The procedure for separation of elastic and inelastic scattering is, in particular, the same. It is based on the fact that, if x_i and ϕ_i are defined as above, if $Y_i=N_i/\phi_i$, where N_i is the counting rate in the ith channel with the telescope at any angle, and if the scattering is a mixture of elastic events and inelastic events involving only the first excited state of the second scatterer, then a plot of Y_i *vs* x_i produces a straight line whose intercept is the elastic yield (denoted by A_0) and whose slope is the inelastic yield (denoted by A_1). The need for accurate knowledge of ϕ_i, which depends on good monitoring of

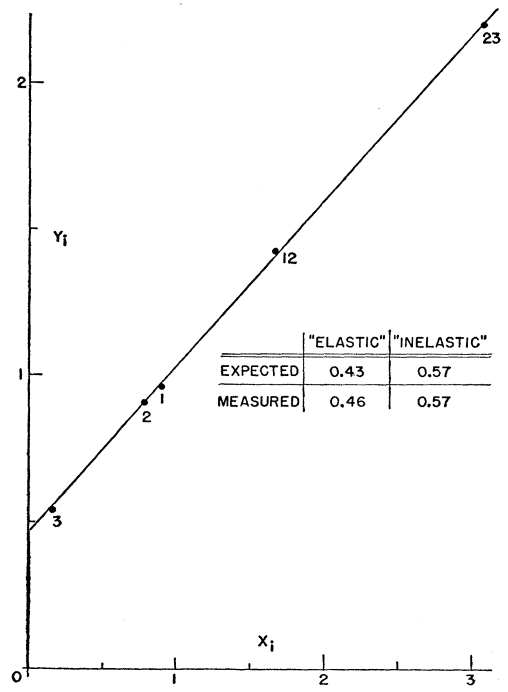

FIG. 7. Observed Y_i-x_i plot in a test run. In small-angle scattering from C^{12}, 57% of the detectible solid angle was covered by a thin absorber in which an additional 4.4 Mev was lost.

the incident energy, becomes apparent when we consider the effect of a small error on the appearance of the Y_i-x_i plot. A hypothetical example of the effect is given in Fig. 6. Here we assume that the true energy corresponds to an absorber thickness R_1 of 2.100 inches, and that the scattering involves a 50% admixture of inelastic events in which 2.4 Mev is lost. The solid line is the plot that should result from a measurement with three counters. Now, if the R_1 chosen for the analysis were larger by 0.010 inch, corresponding to an energy shift of 0.63 Mev, the same measurement would lead to points on the dashed lines; the error in estimating yields would be considerable. The example serves also to show that such an error reveals itself by the failure of points to form a line.

A direct experimental test of the accuracy of the Y_i-x_i plots was carried out in the following way. The telescope was set with $R_1=2.003$ inches and counter separations of 0.065 inch, the spacing appropriate to measurements on C^{12}. Yields and efficiencies were measured for second scattering from C^{12} at 10 degrees to the left. A 0.065-inch copper absorber covering 57% of the scattered beam was then added to R_1; this had the effect of simulating a predictable admixture of inelastic scattering with energy degradation of 4.4 Mev. The

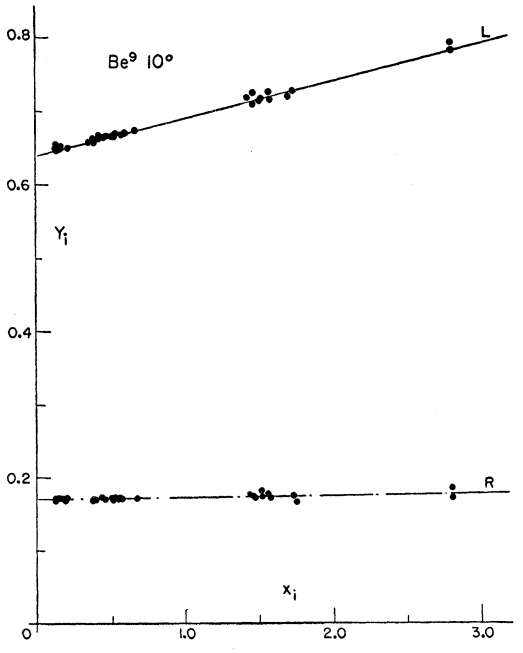

FIG. 8. Y_i-x_i plots for left and right scattering from Be^9 at 10°.

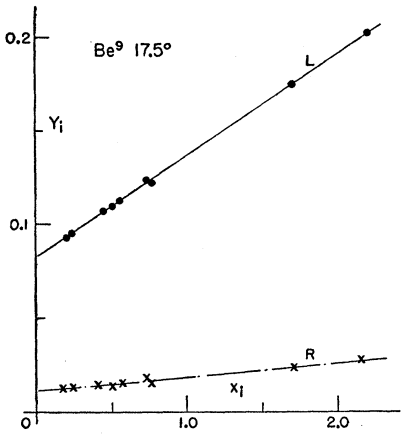

FIG. 9. Y_i-x_i plots for Be^9 at 17.5°.

Y_i-x_i plot derived from the run is shown in Fig. 7; from it one reads an "elastic" yield of 46% and an "inelastic" yield of 57%, with uncertainties of about 2%. The major factor contributing to the accuracy of the result is the relative sharpness of the range curve, which has the effect of producing a much greater spread of ratios x_i than was available to us in earlier work.

EXPERIMENTAL RESULTS

Be^9

The most recent precise study of the level structure of Be^9 has been carried out by Bockelman *et al.*[9] In addition to showing the well-known sharp and prominent level at 2.43 Mev their work confirms the existence of a weakly excited level at 3.05 Mev; a possible level at 1.66 Mev, suggested by other work, appears to be most probably the result of three-body breakup. The reactions studied

[9] Bockelman, Leveque, and Buechner, Phys. Rev. **104**, 456 (1956).

were $Be^9(p,p')Be^9$ and $B^{11}(d,\alpha)Be^9$, with a bombarding energy of 7 Mev. The spectra of inelastic protons at high bombarding energies have not yet been carefully studied. In beginning our asymmetry measurements, we could only guess that the 2.4-Mev level might continue to be responsible for most of the events in which little energy is lost. Contributions from the 3.0-Mev state cannot be resolved by our method, nor can protons in the continuous background covering the same neighborhood of energy. We set up the measurement with thin counters separated by 2.4 Mev at 220 Mev, and anticipated that admixtures of inelastic events with significantly different losses would appear as curvature in our $Y_i - x_i$ plots. The measurements extended from 4 degrees to 37.5 degrees (laboratory), and it is only at the largest angles

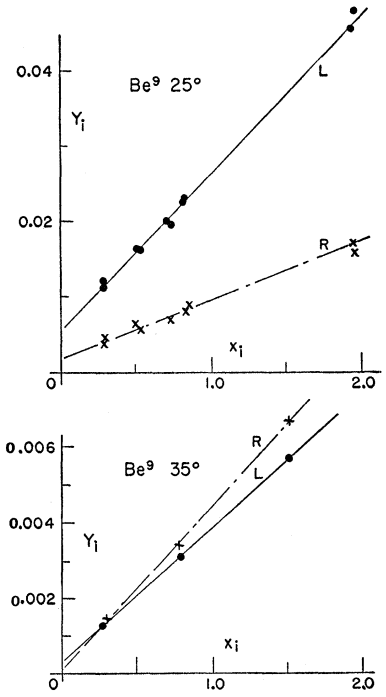

FIG. 10. $Y_i - x_i$ plots for Be^9 at 25° and 35°.

that we have had any difficulty in deciding that the plots are in fact linear.

Typical plots from this run are shown in Figs. 8–10. The data are most extensive at 10 degrees (Fig. 8) since we repeated this measurement frequently for calibration and for tests of consistency. The 10-degree data, as well as those at several other angles, include measurements with both of the counter settings shown in Fig. 3. The Y_i scale of each of the plots is the yield relative to leftward scattering at 6 degrees, the angle at which the standard range curve was obtained.

The angular dependence of yields and polarization in elastic scattering, taken from the intercepts of the $Y_i - x_i$ plots, are shown in Figs. 11 and 12, respectively. The curves included in Fig. 11 are smooth fits to the C^{12} data of CHR, the angular scale having been transformed to take account of the difference in nuclear radius. The vertical scale was adjusted arbitrarily. The C^{12} results are included in order to provide a comparison of relative cross sections for the two nuclei. A qualitative similarity is apparent, and the deviations in the neighborhoods of 20 and 35 degrees ought not to be regarded as necessarily real. The elastic polarization data (Fig.

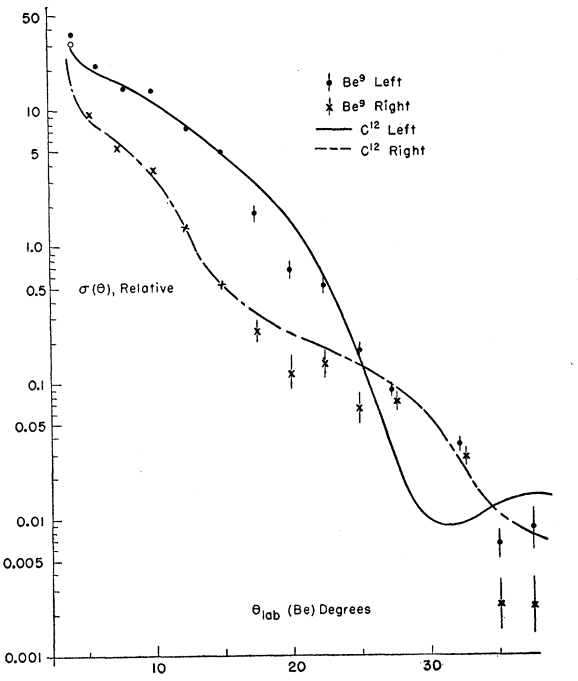

FIG. 11. The points are the left and right elastic yields from Be^9; the curves are the corresponding data from CHR on C^{12}, with angular scale adjusted to the radius of Be^9.

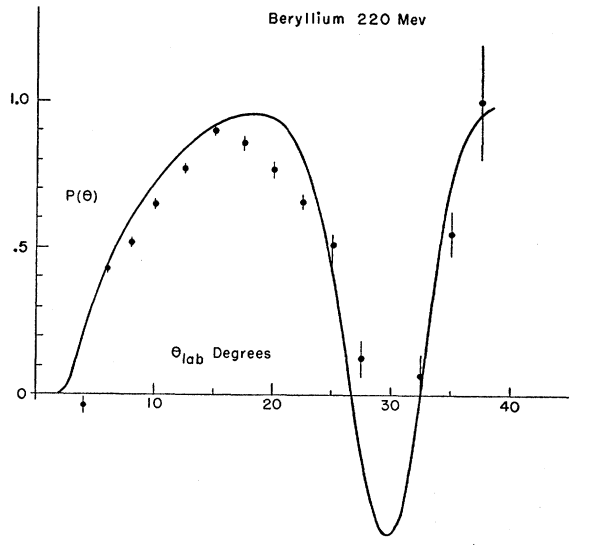

FIG. 12. Polarization in elastic scattering from Be^9. The curve is the prediction from a model adjusted to the polarization data on C^{12}. In this, as in all subsequent theoretical curves, the angular resolution of the counter telescope (Fig. 4) has been accounted for.

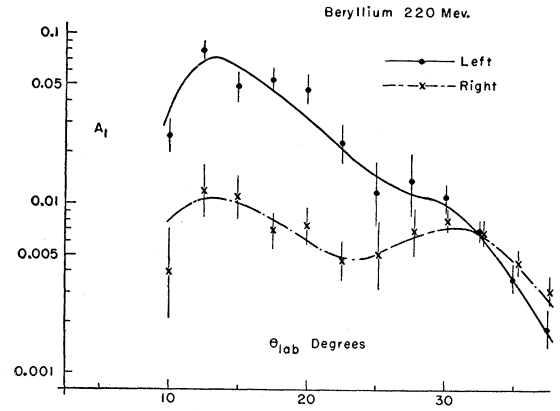

FIG. 13. Left and right inelastic yields from Be^9. It is assumed that the 2.4-Mev state predominates in this process. The curves have no theoretical significance.

12) were obtained from the asymmetries by making use of our knowledge of the first-scattered beam polarization. As often happens in this work, the asymmetries have better precision than do the corresponding yields. Nevertheless, the elastic yields at 30 degrees were so low and so poorly determined that we could make no estimate of the asymmetry at this angle. The curve in Fig. 12 is a theoretical fit, and will be discussed in the next section.

The angular dependence of left and right inelastic yields for Be^9, taken from the slopes of the $Y_i - x_i$ plots, are shown in Fig. 13. The vertical scale is the same as in Fig. 11. We see that, at angles above about 25 degrees, the inelastic process predominates. At large angles, these yields are similar in shape and magnitude to the results on C^{12} reported in CHR; comparison at small angles cannot be made because the earlier work did not have the resolution needed to follow the yields into that region. The curves drawn in Fig. 13 have no theoretical significance, but represent the trends suggested by the data. Polarizations corresponding to these results are discussed in connection with Fig. 17.

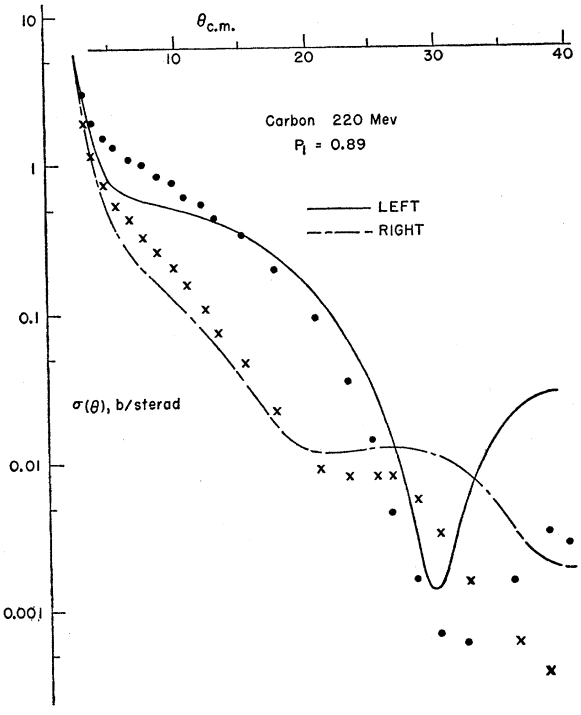

FIG. 14. Left and right elastic yields from C^{12}. The curves are theoretical predictions.

C^{12}

In the present measurements, second scattering from C^{12} was observed only at a few large angles in order to provide checks on results already reported. Agreement was excellent throughout. Figures 14 and 15 display the elastic data of CHR with only minor changes resulting from the remeasurement. They are reproduced here in order to show comparisons with the curves, which are theoretical fits.

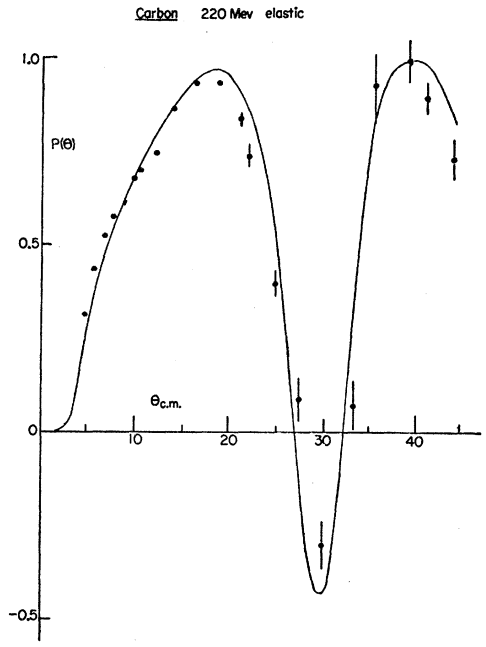

FIG. 15. Polarization in elastic scattering from C^{12}. The model, which was adjusted to fit these data, gives the curve shown.

In Fig. 16, the inelastic asymmetry and polarization data of the Uppsala group[3,4] are compared with the corresponding data of CHR. The angular scale for all results has been adjusted to the common energy of 220 Mev under the assumption that the theorem used in dealing with elastic scattering is equally valid here. Agreement among the three measurements appears to be good, and the curve represents a reasonable fit to all of the data. Figure 17 then compares this curve with the inelastic polarization results obtained for Be^9 in the present work. The angular scale has been adjusted for

nuclear radius in the same way as for elastic scattering. We see a suggestion that, while the processes have similar behavior at large angles, there may be significant differences below 15 degrees.

Al^{27}

The level structure[10] of this nucleus, which exhibits two closely spaced states near 1 Mev, makes the accurate separation of elastic scattering exceedingly difficult by our present methods. Nevertheless, since we wished to obtain at least some data on a nucleus of ground-state spin $\frac{5}{2}$, we set up a measurement on Al^{27} with counter separations of 0.9 Mev, and worked in the

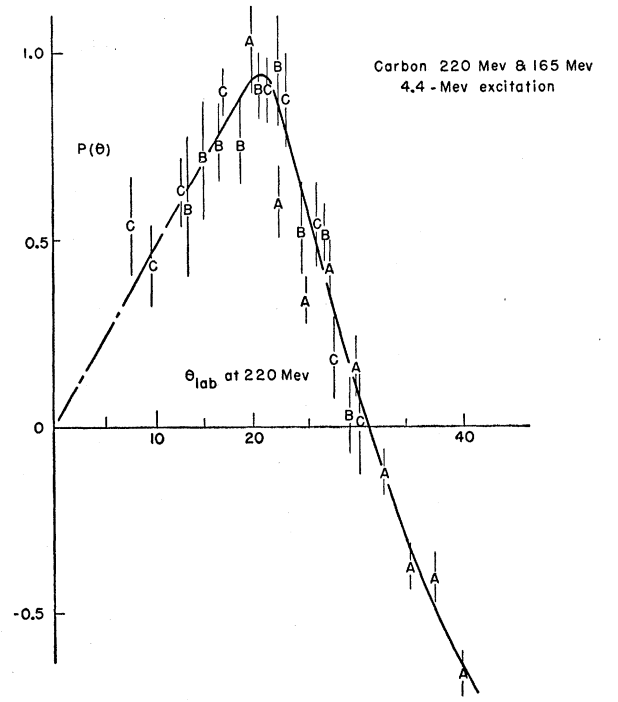

FIG. 16. Polarization in inelastic scattering from C^{12}. Points labeled *A* were obtained from CHR and the present measurement. Points labeled *B* and *C* are quoted from the asymmetry and polarization data of the Uppsala group (references 3 and 4). The curve is drawn as a fit to the data, and has no theoretical basis.

angular region from 8 to 20 degrees. We found no significant changes in channel ratios within this region, and have therefore concluded that inelastic scattering does not play a large role. Figures 18 and 19 show the relative cross sections and the polarizations that were observed; the curves are again theoretical fits.

Ca^{40}

Although the level structure[10] of this nucleus is also complex, the first excited state (3.35 Mev) occurs at an energy high enough to make possible a fairly clean

[10] P. M. Endt and J. C. Kluyver, Revs. Modern Phys. **26**, 95 (1954).

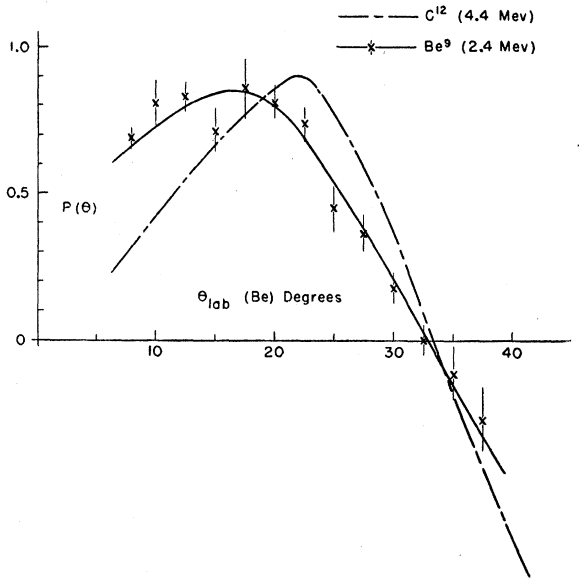

FIG. 17. Polarization in inelastic scattering from Be^9. The points are experimental results. The solid curve is a fit that has no theoretical basis. The dashed curve is drawn, for comparison, from the data of Fig. 16 on C^{12}, after a correction for radius.

separation of elastic scattering. Since the second and third states fall within 0.6 Mev of the first excited state, our measurements of the inelastic scattering represent mixtures to which little significance can be attached. We

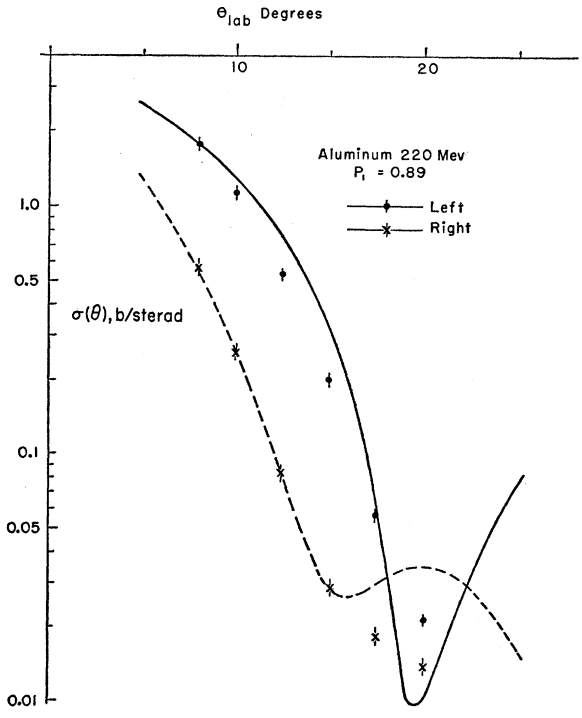

FIG. 18. Left and right yields from Al^{27}. Separation of elastic events has not been attempted for this case. The curves are predictions of the model adjusted to the data of Fig. 15.

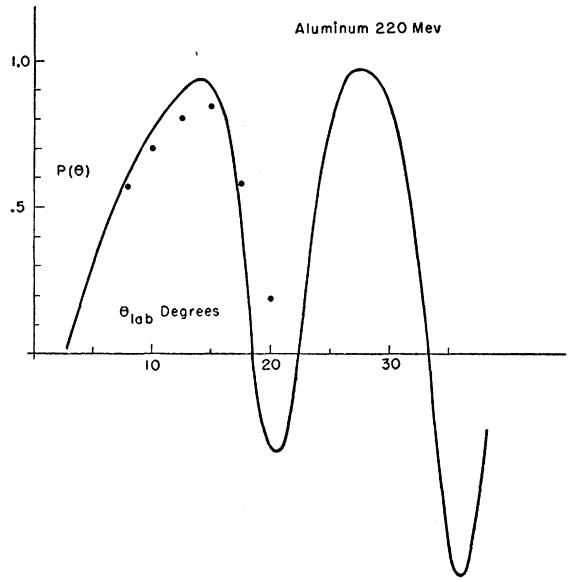

FIG. 19. Polarization in scattering from Al^{27}. The curve is the prediction of the model.

therefore report, in Figs. 20–22, only the results for elastic scattering. The measurements were made with the unregenerated beam and with counters separated by 3.5 Mev. The curves shown in the figures are theoretical fits.

ANALYSIS

Attempts at accounting for the polarization phenomena observed in complex nuclei have been made by many workers,[2] most of whom have attacked the problem by adding a spin-orbit potential to the well-known optical model of nuclear scattering. The result has generally been that, while such calculations reproduce some of the qualitative features of the process, they predict fluctuations in the large-angle polarization that were often not observed. It was pointed out in CHR, however, that much of the discrepancy might have arisen from a failure of many experiments to make satisfactory selection of elastic events; our opinion was based on the observation that, when such selection was made for the case of C^{12}, the results bore a strong resemblance to the predictions of the model. We therefore began a search for a potential that would give a quantitative description of the C^{12} polarization. The present discussion will summarize the results of the search, and will indicate the extent to which the parameters chosen to give the best fit for C^{12} are equally successful in accounting for measurements on the other nuclei that have been studied more recently.

We must assume that most of the details of the model, and of the methods generally used for calculation, are sufficiently familiar not to require discussion here. Apart from some matters that we have not found adequately treated in the literature, and which are collected in appendices to this report, we restrict ourselves to a specification of the notation that we have found convenient and to a brief description of the technique of calculation.

The nuclear potential is taken to be

$$V(r)=-V_1(r)-iV_2(r)+\left(\frac{\hbar}{mc}\right)^2\frac{1}{r}\frac{d[V_3(r)+iV_4(r)]}{dr}\mathbf{l}\cdot\mathbf{s}, \quad (1)$$

where $\mathbf{l}=\mathbf{L}/\hbar$, $\mathbf{s}=\boldsymbol{\sigma}/2$, and m is the proton mass. Signs are chosen so that, when V_1, V_2, and V_3 are positive real functions, the central force is attractive and absorptive, and the spin-orbit force has the same sign as in shell theory. In a partial wave analysis, the state with orbital angular momentum l is subject to the potentials

$$V_l^{\pm}(r)=-V_1(r)-iV_2(r)+\left(\frac{\hbar}{mc}\right)^2\frac{1}{r}\frac{d[V_3(r)+iV_4(r)]}{dr}\begin{bmatrix} l \\ -(l+1)\end{bmatrix}, \quad (2)$$

referring to total angular momenta $l+\frac{1}{2}$ and $l-\frac{1}{2}$, respectively. The nuclear phase shifts, $\delta_{l,n}^{\pm}$, corresponding to these potentials can be computed in WKB approximation.[11] Modified Coulomb phase shifts,[12] $\delta_{l,C}$, for the case of a uniformly charged sphere of radius r_1 are added to the nuclear phase shifts; each pair of total phase shifts is equivalent to the quantities $(\eta_l+\delta_l^{\pm})$ defined in

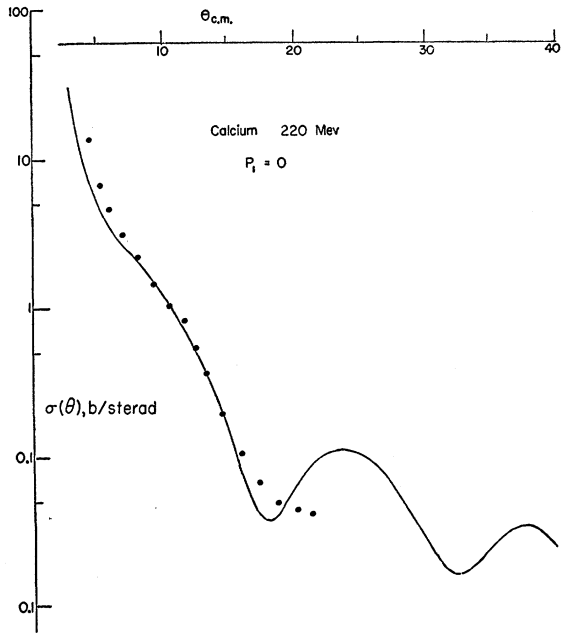

FIG. 20. Unpolarized elastic cross section for Ca^{40}. The curve is the prediction of the model.

[11] N. F. Mott and H. S. W. Massey, *Theory of Atomic Collisions* (Clarendon Press, Oxford, 1949), second edition, p. 127.
[12] K. M. Gatha and R. J. Riddell, Phys. Rev. **86**, 1035 (1952).

Appendix A. Equations (A9), (A12), and (A13) of that appendix are then used to give amplitudes, polarization, and differential cross sections for the scattering.

In most of our calculations we have used potential shapes of the type suggested by Woods and Saxon[13] and used originally in the polarization calculations of Sternheimer.[14] Thus, for example, we take

$$V_1(r)=V_1(0)/\{1+\exp[(r-r_0)/a]\}, \qquad (3)$$

and assume that the parameters r_0 and a are the same for all functions appearing in Eq. (1).

It is shown in Appendix B that, to a good approximation, the parameter k_1 of the optical model is related to the potential V_1 by

$$k_1=(\epsilon_c k_c/p_c^2c^2)V_1, \qquad (4)$$

where ϵ_c, k_c, and p_c are, respectively, the total energy, wave number, and momentum of the proton in center-of-momentum coordinates. The optical parameter $k_2=\frac{1}{2}K$ can be related to the potential V_2 in the same way. It can, however, be estimated directly[15] from a knowledge of experimental nucleon-nucleon cross sections. Assuming, for example, an effective nuclear radius of 2.52 f (1 f≡1 fermi≡10^{-13} cm) for C^{12}, we arrive at the value $k_2=0.215$ f^{-1}. This number has been used in many of our calculations, including those that we regard as the best fits.

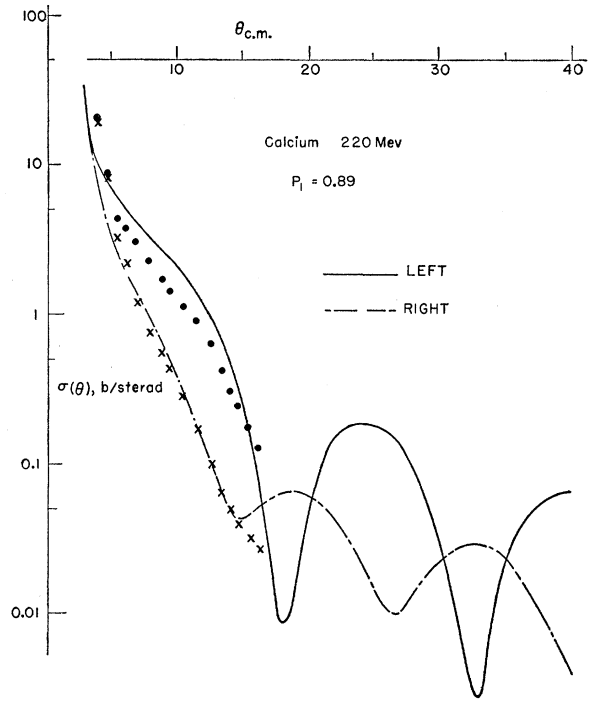

FIG. 21. Left and right elastic yields from Ca^{40}. The curves are the predictions of the model.

[13] R. D. Woods and D. S. Saxon, Phys. Rev. **95**, 577 (1954).
[14] R. M. Sternheimer, Phys. Rev. **97**, 1314 (1955).
[15] J. M. Cassel and J. D. Lawson, Proc. Phys. Soc. (London) **A67**, 125 (1954).

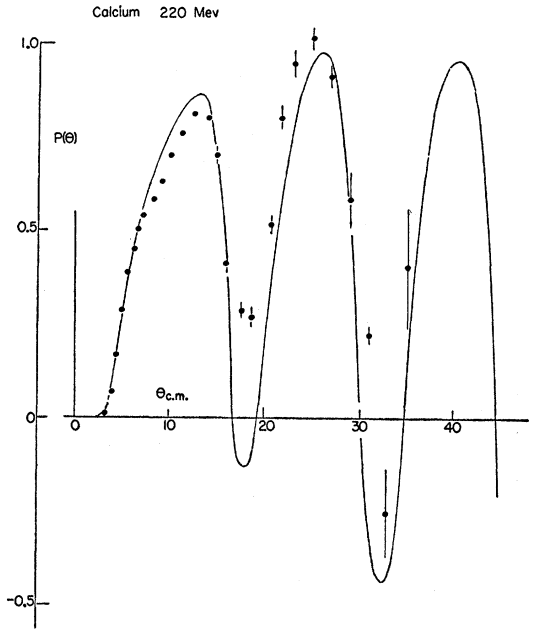

FIG. 22. Polarization in elastic scattering from Ca^{40}. The curve is the prediction of the model.

When the Woods-Saxon shape for the potentials is chosen, the Thomas spin-orbit coupling gives the explicit potential

$$V_{s.o.}(r)=-\left(\frac{\hbar}{mc}\right)^2\frac{V_3(0)+iV_4(0)}{a}\frac{e^{(r-r_0)/a}}{r[1+e^{(r-r_0)/a}]^2}. \qquad (5)$$

If the spin-orbit effect arose from Thomas precession alone, one would expect[2] the strength of this potential to be one-half that of the central potential. We find, in agreement with others, that it must be in fact many times larger.

The entire computation outlined above was programed for an IBM-650 digital computer. An interpretive system was used, and we found that a calculation involving 10 l values needed a computing time of about 15 minutes in order to print out data at 15 angles. The slowness of the program prevented us from demanding that the machine carry out a systematic search for best fits; instead, we varied the free parameters of the model more or less at random, attempting to discover trends that would assist us in converging toward the best values. A sequence of about fifty runs was devoted to a study of the C^{12} scattering before any attempt was made to extend the model to other nuclei. We discovered rather quickly that the large-angle polarization in C^{12} could be fitted accurately for a wide variety of potential strengths, provided that the effective nuclear radius was in the neighborhood of 2.5 fermis. But great difficulty was encountered in arriving at a good description of the scattering below the first polarization maximum, the region where Coulomb effects are strong. We found

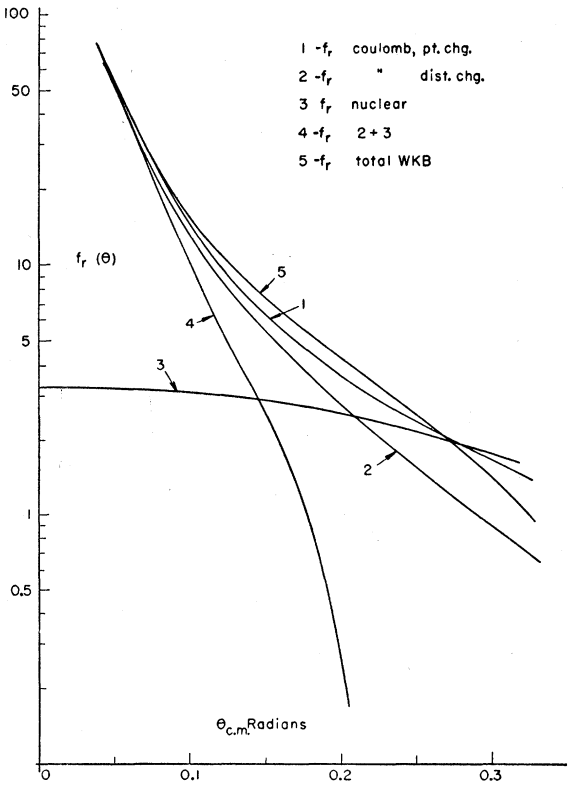

FIG. 23. Behavior of the small-angle scattering amplitude $f_r(\theta)$ for C^{12}.

almost invariably that, if the large-angle polarization was accurately given, the small-angle prediction rose too rapidly and produced a maximum that was too broad. Finally, a sequence of runs in which the shape parameter a was reduced led us to the conclusion that the best fits are obtained with this length no greater than 0.1 fermi; it had initially been maintained at about 0.4 fermi, in rough conformity with what is known from the results of high-energy electron scattering.

The nuclear parameters that gave the C^{12} curves reproduced in Figs. 14 and 15 were as follows: $r_0=2.4$ fermis, $a=0.1$ fermi, $r_1=2.5$ fermis, $[(r_0+a)/A^{\frac{1}{3}}=1.09$ fermis$]$, $k_1(0)=0.086$ f^{-1}, $[V_1(0)=10$ Mev$]$, $k_2(0)=0.215$ f^{-1}, $[V_2(0)=25$ Mev$]$, $V_3(0)=225$ Mev, $V_4(0)=0$. When this set had been fixed upon, we ran Be^9, Al^{27}, and Ca^{40} with the same potential, changing only r_0 so as to maintain the relation with A given above; the Coulomb parameters were, of course, also changed. The results of these runs are the curves reproduced in Figs. 12 and 18–22. One sees that the fits are, in most respects, as good for these nuclei as for C^{12}. We are fairly confident that, within the framework of the model adopted here, no significant improvement in these calculations would result from further adjustment of the parameters. What we cannot say with as much confidence is that our set of parameters is unique.

The computed scattering amplitudes at small angles for the case of C^{12} are given in Figs. 23–25. We include the amplitudes for pure Coulomb scattering (with point charge and with distributed charge), for pure nuclear scattering, and for combined nuclear and Coulomb scattering (with distributed charge). The combination is made in each of two ways: by taking the sum of the separate amplitudes, and by using combined phase shifts according to the method of Appendix A. The calculations made by the latter method are labeled "total WKB." If the two procedures were equivalent, curves 4 and 5 in Figs. 23 and 24 would coincide, as would the two pairs of curves in Fig. 25. We notice that, although the amplitudes f_i and g_r meet this test, f_r and

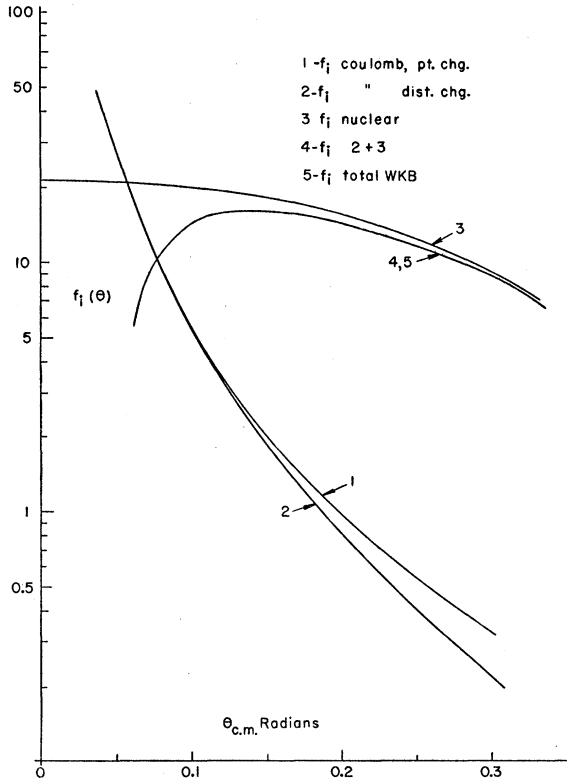

FIG. 24. Behavior of the small-angle scattering amplitude $f_i(\theta)$ for C^{12}.

g_i do not. Thus we have been led to suspect that there may be large discrepancies between small-angle results calculated in Born approximation and those found by the WKB phase-shift procedure used in most of our work. We have therefore carried out comparisons of the two approximations at small angles. The nuclear model used for the comparison was a square well whose radius and depth parameters were closely equivalent to those of the most successful Woods-Saxon model. The scattering amplitudes computed this way exhibited the same discrepancies as those revealed by the test already mentioned; indeed f_r and g_i were found to be significantly different even for the case of pure nuclear

scattering. Figures 26 and 27 show cross sections and polarizations computed in both approximations.[16] We note that the cross sections in pure nuclear scattering are in fair agreement; all other comparisons exhibit large differences. In making these calculations for the case in which Coulomb scattering is included, we took account of the electromagnetic interaction[2] between the proton moment and the nuclear charge. This term had been omitted in our previous work, but we have observed that its effect is not large. It is particularly interesting to see that the proton polarization in Born approximation (curve 3 of Fig. 27) at small angles shows a striking similarity to the characteristic experimental shape observed in almost all measurements; the WKB phase shift calculations have consistently failed to describe this feature of the data. We are thus led to the suggestion that Born approximation is the more valid

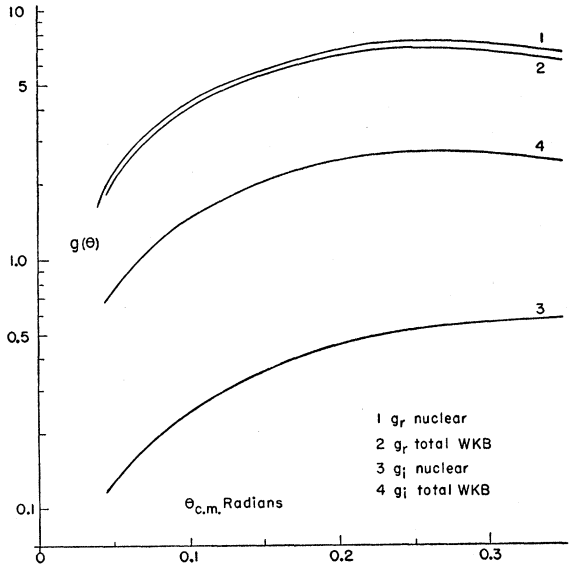

FIG. 25. Behavior of the small-angle scattering amplitudes $g_r(\theta)$ and $g_i(\theta)$ for C^{12}.

procedure in the small-angle region, even though it fails qualitatively at large angles. The WKB approximation has given successful fits to the large-angle polarization, but fails to describe cross sections beyond the first diffraction minimum.

We have found that all methods of calculation lead, in the case of C^{12}, to the same value of $f_i(0)$ for nuclear scattering. It is then interesting to see whether this value predicts, through the optical theorem, the correct neutron total cross section. The agreement with experiment is in fact good: the prediction of 289 mb is to be compared with the measured value of 294±3 mb, taken as the weighted mean of the two neutron total cross-

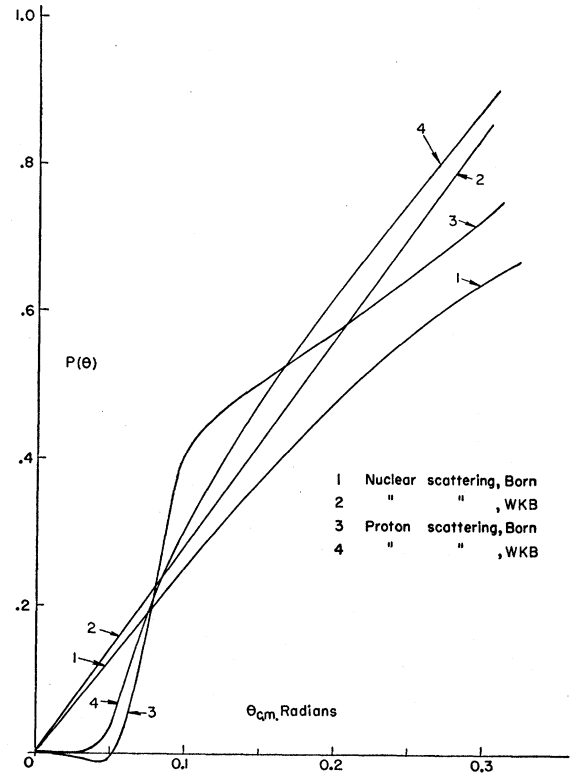

FIG. 26. Cross sections for C^{12} in WKB and Born approximations.

section measurements[17,18] that have been carried out at 220 Mev. The agreement between computed and measured total cross sections persists for the heavier nuclei, as shown in Fig. 28, provided we consider only the prediction from the WKB calculation; the corresponding

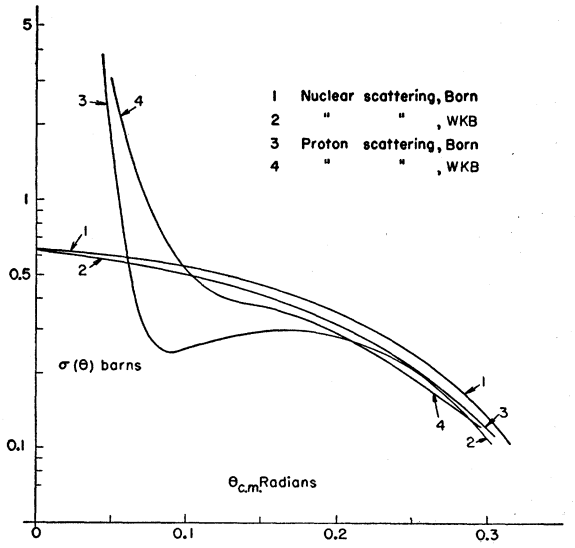

FIG. 27. Polarizations for C^{12} in WKB and Born approximations.

[16] The proton calculations in "Born approximation" were made by adding *exact* point-charge Coulomb amplitudes to nuclear and magnetic-moment amplitudes taken in strict Born approximation.

[17] J. DeJuren and B. J. Moyer, Phys. Rev. **81**, 919 (1951).
[18] Mott, Guernsey, and Nelson, Phys. Rev. **88**, 9 (1952).

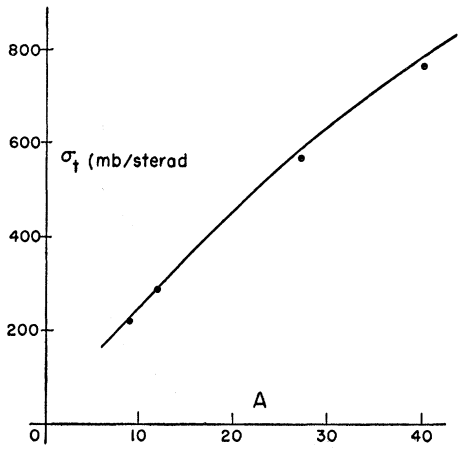

FIG. 28. Total cross sections for neutron scattering. The curve is an interpolation of the available experimental data. The four points are the predictions of the present model, obtained from the optical theorem and the amplitudes $f_i(0)$ computed in WKB approximation.

prediction in Born approximation rises much too rapidly with nuclear radius.

The cross sections for absorption depend, in this model, on nuclear radius and on the imaginary potential. The predictions, which are rather free from ambiguity, are consistently about 30% too low in comparison with interpolations from data[15] at other energies. Agreement can be produced by increasing r_0 to $1.3A^{\frac{1}{3}}$ fermis, but it appears to be impossible to make this change and at the same time to maintain our descriptions of the polarization patterns and the total cross sections. Perhaps it should be emphasized, however, that we have chosen $V_4=0$ as adequate for the polarization fits; an extended study of the effect of this term might resolve the difficulties with absorption cross sections.

In summary, we can make the following statements about the results of our analysis:

(i) Parameters for the optical model with spin-orbit coupling can be found such that, in partial-wave analysis using WKB approximations to the nuclear phase shifts, accurate descriptions of polarization are given for four nuclei.

(ii) The agreement with experimental data on Be^9 and Al^{27} is sufficiently good to suggest that the nonzero ground-state spins of these nuclei have no large effect on the polarization in elastic scattering.

(iii) The WKB predictions of polarization at small angles are consistently too smooth. In Born approximation at small angles, however, the observed shape of the function appears to be given correctly.

(iv) In order to achieve good fits to the polarization, it has been found necessary to use nuclear distributions with sharp tails.

(v) The relative differential cross sections are well described by the model, at angles below the first minimum; at larger angles, the model predicts too much scattering.

(vi) Total cross sections are accurately given by the optical theorem when the scattering amplitude in WKB approximation is used. Absorption cross sections are, however, consistently underestimated by potentials in which an imaginary spin-orbit term is not present.

ACKNOWLEDGMENTS

The assistance of Dr. A. Roberts, Dr. J. H. Tinlot, Dr. W. G. Chesnut, Dr. S. Spital, Dr. D. Cohen, Mr. R. S. Harding, Mr. K. Gotow, and other members of our research group is gratefully acknowledged. Mr. W. Gibson is responsible for most of the work involved in programing the calculations and in developing Appendix A. The help of Dr. K. J. Le Couteur and Mrs. E. Mandl was invaluable in the design of the regenerator, and that of Mr. J. Dungan in its construction; the suggestion that a regenerator be used for experiments of this kind was made originally by Dr. Richard Wilson.

APPENDIX A

We establish here the connections between scattering amplitudes and phase shifts for the elastic scattering of protons by spinless nuclei. Since a Hamiltonian involving a potential of the type given in Eq. (1) commutes with J^2 and J_z, their respective eigenvalues j and m are good quantum numbers. The wave function in the (j,m) representation is expanded in terms of the (l,s,m_l,m_s) representation by means of Clebsch-Gordan coefficients. Thus,

$$\psi(j,m)=\sum_{m_l,m_s}\phi(m_l,m_s)(m_l,m_s|\,j,m), \qquad \text{(A1)}$$

with $m=m_l+m_s$. We can also write

$$\phi(m_l,m_s)=R_l^{\pm}(r)Y_l^m(\theta,\varphi)\chi_s^{m_s}. \qquad \text{(A2)}$$

$R_l^{\pm}$ is the radial function for $j=l\pm\frac{1}{2}$; $\chi_s^{m_s}$ are spin eigenfunctions for the proton.

We choose coordinates so that the incident beam is moving along the positive z axis. A beam completely polarized in the positive z direction[19] has $m=0$ and $m=m_s=\frac{1}{2}$ before scattering. From this fact, and from (1) and (2), we have

$$\psi(j,\tfrac{1}{2})=\frac{R_l^+}{(4\pi)^{\frac{1}{2}}}\left[(l+1)^{\frac{1}{2}}P_l^0(\cos\theta)\chi_{\frac{1}{2}}^{\frac{1}{2}}+\frac{e^{i\varphi}}{(l+1)^{\frac{1}{2}}}P_l^1(\cos\theta)\chi_{\frac{1}{2}}^{-\frac{1}{2}}\right]+\frac{R_l^-}{(4\pi)^{\frac{1}{2}}}\left[-l^{\frac{1}{2}}P_l^0(\cos\theta)\chi_{\frac{1}{2}}^{\frac{1}{2}}+\frac{e^{i\varphi}}{l^{\frac{1}{2}}}P_l^1(\cos\theta)\chi_{\frac{1}{2}}^{-\frac{1}{2}}\right] \qquad \text{(A3)}$$

[19] The choice of spin direction represented by the spin eigenfunctions is arbitrary; the two functions form a complete set, and any polarization can be represented in terms of them. However, we note that, while "spin flip" cannot occur for spin perpendicular to the direction of motion in the case of a spinless nucleus, it can occur for spin parallel or antiparallel to the direction of motion.

for each l value involved in the scattering. The radial functions have asymptotic forms

$$R_l^{\pm}\sim\frac{C_l^{\pm}}{kr}\sin(kr-\tfrac{1}{2}l\pi-n\ln 2kr+\eta_l+\delta_l^{\pm}), \quad \text{(A4)}$$

where $n=Ze^2/\hbar v$, and $\delta_l^{\pm}$ are deviations from the point-charge Coulomb phase shifts η_l. The total wave has asymptotic form

$$\psi\sim e^{i[kz-n\ln k(r-z)]}\chi_{\frac{1}{2}}^{\frac{1}{2}}+f(\theta)\frac{e^{i\beta}}{kr}\chi_{\frac{1}{2}}^{\frac{1}{2}}+g(\theta,\varphi)\frac{e^{i\beta}}{kr}\chi_{\frac{1}{2}}^{-\frac{1}{2}}, \quad \text{(A5)}$$

where $\beta=kr-n\ln 2kr$. It is convenient to write

$$f(\theta)=f_n(\theta)+f_C(\theta), \quad \text{(A6)}$$

where $f_n(\theta)$ is the deviation of $f(\theta)$ from the point-charge Coulomb amplitude, $f_C(\theta)$, that arises from the defining relation

$$\sum_l\frac{(2l+1)}{kr}\exp(i\eta_l)i^l\sin(\beta-\tfrac{1}{2}l\pi+\eta_l)\chi_{\frac{1}{2}}^{\frac{1}{2}}P_l^0(\cos\theta)$$
$$=e^{i[kz-n\ln k(r-z)]}\chi_{\frac{1}{2}}^{\frac{1}{2}}+f_C(\theta)\frac{e^{i\beta}}{kr}\chi_{\frac{1}{2}}^{\frac{1}{2}}. \quad \text{(A7)}$$

We now manipulate these equations in the following way. Substitute (A4) into (A3), sum over l, and identify the result with the left-hand side of (A5). Then subtract (A7) from (A5) and, in the resulting identity, equate successively the coefficients of $e^{i\beta}\chi_{\frac{1}{2}}^{\frac{1}{2}}$, $e^{-i\beta}\chi_{\frac{1}{2}}^{\frac{1}{2}}$, $e^{i\beta}\chi_{\frac{1}{2}}^{-\frac{1}{2}}$, and $e^{-i\beta}\chi_{\frac{1}{2}}^{-\frac{1}{2}}$. This work yields four identities:

$$C_l^{+}=[4\pi(l+1)]^{\frac{1}{2}}\exp[i(\eta_l+\delta_l^{+}+\tfrac{1}{2}l\pi)], \quad \text{(A8)}$$
$$C_l^{-}=-(4\pi l)^{\frac{1}{2}}\exp[i(\eta_l+\delta_l^{-}+\tfrac{1}{2}l\pi)],$$

and

$$f_n(\theta)=\frac{1}{2i}\sum_l\{(l+1)\{\exp[2i(\eta_l+\delta_l^{+})]-\exp[2i\eta_l]\}$$
$$+l\{\exp[2i(\eta_l+\delta_l^{-})]-\exp[2i\eta_l]\}\}P_l^0,$$
$$g(\theta,\varphi)=\frac{1}{2i}\sum_l\{\exp[2i(\eta_l+\delta_l^{+})]-\exp[2i(\eta_l+\delta_l^{-})]\}e^{i\varphi}P_l^1 \quad \text{(A9)}$$
$$\equiv g_0(\theta)e^{i\varphi}.$$

$g_0e^{i\varphi}$ and f are the amplitudes for scattering with and without spin flip, for protons with incident spin along $+z$. The corresponding amplitudes for protons with opposite incident spin are $-g_0e^{-i\varphi}$ and f, respectively. We can then construct the scattering matrix

$$M=\begin{pmatrix} f & -g_0e^{-i\varphi} \\ g_0e^{i\varphi} & f \end{pmatrix}. \quad \text{(A10)}$$

Finally, we can write yields and polarizations from well-known theorems. Starting with an unpolarized beam, we find for the intensity after one scattering

$$I_1^0=\tfrac{1}{2}\,\mathrm{Tr}(M_1M_1^{\dagger})=f_1^2+g_1^2,$$

and, for the polarization,

$$\langle\boldsymbol{\sigma}_1\rangle=\mathrm{Tr}(M_1M_1^{\dagger}\boldsymbol{\sigma})/\mathrm{Tr}(M_1M_1^{\dagger}). \quad \text{(A11)}$$

If the normal to the first scattering plane is $\mathbf{j}_1$, a unit vector parallel to y_1, then $\varphi_1=0$ and we find a polarization[20]

$$\langle\boldsymbol{\sigma}_1\rangle=\frac{2\,\mathrm{Im}f_1^{*}g_1}{f_1^2+g_1^2}\mathbf{j}_1\equiv P_1\mathbf{j}_1. \quad \text{(A12)}$$

The intensity after a second scattering of this beam is

$$I_2=\tfrac{1}{2}[\mathrm{Tr}(M_2M_2^{\dagger})+\langle\boldsymbol{\sigma}_1\rangle\cdot\mathrm{Tr}(M_2\boldsymbol{\sigma}M_2^{\dagger})].$$

If $\mathbf{j}_2$, a unit vector normal to the plane of second scattering, is parallel to y_2, then $\varphi_2=0$ and we find that

$$I_2=I_2^0(1+P_1P_2\mathbf{j}_1\cdot\mathbf{j}_2), \quad \text{(A13)}$$

where P_2 is identical in form with P_1, and represents the polarization that would arise in second scattering if the incident beam were unpolarized.

APPENDIX B

Assembled here are formulas that we have found useful in interpreting experimental data with the optical model. First, consider the relativistic kinematics of the elastic scattering of a proton (mass m, momentum p, velocity βc) by a nucleus (mass M) at rest in the laboratory. The total energy of the system in the laboratory is

$$E=\gamma mc^2+Mc^2, \quad \text{(B1)}$$

where $\gamma^{-2}=1-\beta^2$. The velocity of the center of momentum (c.m.) is given by

$$\beta_0=pc/E, \quad \text{(B2)}$$

and the total energy in the c.m. system is

$$E_0=E/\gamma_0. \quad \text{(B3)}$$

If $k=p/\hbar$ is the wave number of the proton in laboratory coordinates, then in the c.m. system it becomes

$$k_c=(Mc^2/E_0)k. \quad \text{(B4)}$$

(A convenient factor connecting k with p is given by

$$k=5.0680\times10^{10}pc\ \mathrm{cm}^{-1},$$

[20] The sign of the polarization computed from (9) and (12) is positive or negative depending on whether $\langle\boldsymbol{\sigma}\rangle$ is parallel or antiparallel to the vector $\mathbf{n}=\mathbf{k}_f\times\mathbf{k}_i$, i and f referring to the incident and scattered beams, respectively. This is opposite to the convention adopted by most experimentalists, who refer to the vector $\mathbf{k}_i\times\mathbf{k}_f$. We perpetuate this unfortunate confusion by reporting our computed polarizations according to the latter convention.

TABLE I. Coulomb phase shifts for C^{12}.

l	η_l	$n\ln(l+\frac{1}{2})$	$\delta_{l,C}$
0	−0.0430	−0.0518	0.1130
1	0.0316	0.0303	0.1145
2	0.0689	0.0684	0.1175
3	0.0938	0.0936	0.1219
4	0.1125	0.1123	0.1276
5	0.1274	0.1273	0.1345
6	0.1399	0.1399	0.1424
7	0.1505	0.1505	0.1510
8	0.1599	0.1599	0.1599

where pc is in Mev). Now let θ_l and φ_l be the laboratory angles for scattering and recoil, respectively, and let θ be the c.m. scattering angle. Then we have

$$\tan\theta_l=(\sin\theta/\gamma_0)[(m/M)(m+M\gamma)/(m\gamma+M)+\cos\theta]^{-1}, \quad \text{(B5)}$$

and

$$\tan\varphi_l=(\sin\theta/\gamma_0)/(1+\cos\theta). \quad \text{(B6)}$$

If a reduced mass, μ, for the proton is defined so that $\beta\gamma\mu c=\beta_c\gamma_c mc$, then it becomes

$$\mu=\gamma_0 mM/(\gamma m+M) \quad \text{(B7)}$$

and the total energy of the *proton* in the c.m. system is

$$\epsilon_c=\gamma\mu c^2. \quad \text{(B8)}$$

The optical parameter k_1 is given by

$$\frac{k_1}{k_c}=\left[\frac{(\epsilon_c+V_1)^2-\mu^2c^4}{\epsilon_0{}^2-\mu^2c^4}\right]^{\frac{1}{2}}-1\cong\frac{V_1\epsilon_c}{p_c{}^2c^2}, \quad \text{(B9)}$$

where $-V_1$ is, as in Eq. (1), the real part of the central nuclear potential. The error made in using the approximation is less than 2% for our parameters.

In the treatment of Coulomb scattering, the point-charge phase shifts are

$$\eta_l=\arg\Gamma(1+l+in)$$
$$=-nC+\sum_{k=1}^{\infty}\left[\frac{n}{k}-\tan^{-1}\left(\frac{n}{l+k}\right)\right] \quad \text{(B10)}$$
$$\cong n\ln(l+\tfrac{1}{2}),$$

where $C=0.57722\cdots$ and $n=Ze^2/\hbar v=Z/137\beta$. The recursion relation,

$$\eta_l-\eta_{l-1}=\tan^{-1}(n/l),$$

is always useful, but the series in (B10) is only convenient when it is rapidly convergent. Table I compares the exact point-charge Coulomb phase shifts for 220-Mev protons on C^{12} with the approximation given above, and with the modified phase shifts[12] $\delta_{l,C}$, computed for $kr_1=8.58$. The third column indicates that the approximation is good at all but the first few l values.